Energy & Environmental Science

Cite this: *Energy Environ. Sci.*, 2012, **5**, 7606

www.rsc.org/ees

PAPER

Water-soluble mononuclear cobalt complexes with organic ligands acting as precatalysts for efficient photocatalytic water oxidation†

Dachao Hong,[a] Jieun Jung,[a] Jiyun Park,[b] Yusuke Yamada,[a] Tomoyoshi Suenobu,[a] Yong-Min Lee,[b] Wonwoo Nam*[b] and Shunichi Fukuzumi*[ab]

Received 21st January 2012, Accepted 29th March 2012
DOI: 10.1039/c2ee21185h

The photocatalytic water oxidation to evolve O_2 was performed by photoirradiation ($\lambda > 420$ nm) of an aqueous solution containing $[Ru(bpy)_3]^{2+}$ (bpy = 2,2′-bipyridine), $Na_2S_2O_8$ and water-soluble cobalt complexes with various organic ligands as precatalysts in the pH range of 6.0–10. The turnover numbers (TONs) based on the amount of Co for the photocatalytic O_2 evolution with $[Co^{II}(Me_6tren)(OH_2)]^{2+}$ (**1**) and $[Co^{III}(Cp^*)(bpy)(OH_2)]^{2+}$ (**2**) [Me_6tren = tris(*N*,*N*′-dimethylaminoethyl) amine, Cp^* = η^5-pentamethylcyclopentadienyl] at pH 9.0 reached 420 and 320, respectively. The evolved O_2 yield increased in proportion to concentrations of precatalysts **1** and **2** up to 0.10 mM. However, the O_2 yield dramatically decreased when the concentration of precatalysts **1** and **2** exceeded 0.10 mM. When the concentration of $Na_2S_2O_8$ was increased from 10 mM to 50 mM, CO_2 evolution was observed during the photocatalytic water oxidation. These results indicate that a part of the organic ligands of **1** and **2** were oxidized to evolve CO_2 during the photocatalytic reaction. The degradation of complex **2** under photocatalytic conditions and the oxidation of Me_6tren ligand of **1** by $[Ru(bpy)_3]^{3+}$ were confirmed by ^1H NMR measurements. Dynamic light scattering (DLS) experiments indicate the formation of particles with diameters of around 20 ± 10 nm and 200 ± 100 nm during the photocatalytic water oxidation with **1** and **2**, respectively. The particle sizes determined by DLS agreed with those of the secondary particles observed by TEM. The XPS measurements of the formed particles suggest that the surface of the particles is covered with cobalt hydroxides, which could be converted to active species containing high-valent cobalt ions during the photocatalytic water oxidation. The recovered nanoparticles produced from **1** act as a robust catalyst for the photocatalytic water oxidation.

[a]*Department of Material and Life Science, Division of Advanced Science and Biotechnology, Graduate School of Engineering, Osaka University, ALCA, Japan Science and Technology Agency (JST), Suita, Osaka 565-0871, Japan. E-mail: fukuzumi@chem.eng.osaka-u.ac.jp; Fax: +81-6-6879-7370; Tel: +81-6-6879-7368*
[b]*Department of Bioinspired Science, Ewha Womans University, Seoul 120-750, Korea. E-mail: wwnam@ewha.ac.kr*

† Electronic supplementary information (ESI) available: Synthesis of cobalt complexes (Page S2), coexisting effect of Cl^- ion on O_2 evolution (Fig. S1), generation of $[Ru(bpy)_3]^{3+}$ (Fig. S2), $H_2{}^{18}O$ labeling experiment (Fig. S3), repeated O_2 evolution at pH 8.0 (Fig. S4), ^1H NMR spectra of **2** (Fig. S5), oxidation of organic ligands with $[Ru^{III}(bpy)_3]^{3+}$ detected by UV-vis (Fig. S6), powder XRD spectra of particles (Fig. S7), TG/DTA for nanoparticles (Fig. S8) and dependence of O_2 evolution on $[Ru(bpy)_3]^{2+}$ concentration (Fig. S9). See DOI: 10.1039/c2ee21185h

Broader context

Artificial photosynthesis using sunlight is one of the most promising systems to achieve a sustainable energy cycle, where water is oxidized to O_2 to supply electrons. The development of efficient water oxidation catalysts driven by visible light is the most challenging research topic in artificial photosynthesis. Here, we employ mononuclear cobalt complexes with organic ligands as precatalysts for light-driven water oxidation using a photosensitizer and an electron acceptor. The actual catalysts for the photocatalytic water oxidation derived from the cobalt complexes were revealed to be nanoparticles covered with cobalt hydroxides on the surface. Thus, an appropriate choice of organic ligands enables us to attain highly active catalysts for water oxidation.

1. Introduction

Solar energy is used efficiently to produce high-energy chemicals such as sugar by photosynthesis, in which an oxygen-evolving complex composed of a manganese-oxo cluster with a calcium ion oxidizes water to extract electrons and protons.[1–6] In order to mimic the photosynthesis artificially, light-harvesting and charge-separation units as well as catalytic units for water oxidation and CO_2 fixation should be developed.[7–17] To date, the development of efficient water oxidation catalysts (WOCs) is a bottleneck to attain artificial photosynthesis because water oxidation is a challenging process including multi-electron transfer coupled with multi-proton transfer.[18–22]

For the past few decades, extensive efforts have been devoted to develop WOCs using various metal complexes.[23–50] Many multi- or mononuclear ruthenium complexes with organic ligands have been demonstrated to act as WOCs since the finding of a binuclear ruthenium complex, the so-called "blue dimer", which catalyses the water oxidation by an oxidant such as ammonium cerium nitrate.[51–66] Iridium complexes have also been demonstrated as effective WOCs in later years, such as mononuclear iridium complexes with a Cp^* (Cp^* = η^5-pentamethylcyclopentadienyl) ligand.[67–74] However, the drawbacks of these precious metals are high prices and limited stock for any practical applications.

Recently, cobalt-based compounds have attracted many researchers, because cobalt is much more abundant and less expensive than ruthenium and iridium.[75–86] For example, a thin film of cobalt phosphate prepared by electrodeposition exhibits low overpotential and high catalytic reactivity for water oxidation.[81,82] Co_3O_4 has also been reported to act as an active catalyst in the heterogeneous photocatalytic water oxidation with $[Ru(bpy)_3]^{2+}$ (bpy = 2,2′-bipyridine) as a photosensitizer and $Na_2S_2O_8$ as a sacrificial electron acceptor.[16,76] Besides the electrochemical and the photocatalytic water oxidation, thermal water oxidation can be catalysed by WOCs containing Co(II) ions with a one-electron oxidant such as $[Ru(bpy)_3]^{3+}$.[77–80] Thus, cobalt-containing materials are promising candidates for WOCs in developing artificial photosynthesis.

On the perspective of cobalt complexes, mononuclear cobalt complexes with organic ligands are attractive candidates, because catalytically active cobalt ions can be isolated on the atomic level and their reactivity can be controlled by changing the chemical structure of ligands as far as they are stable under highly oxidative conditions. A tetranuclear cobalt polyoxometalate complex of $[Co^{II}_4(H_2O)_2(\alpha\text{-}PW_9O_{34})_2]^{10-}$, which contains no organic ligand, has been reported to act as an efficient catalyst in the homogenous photocatalytic system using $[Ru(bpy)_3]^{2+}$ and $Na_2S_2O_8$.[83] Although it has recently been reported that the tetranuclear cobalt polyoxometalate complex decomposed at pH 8.0 in the electrochemical water oxidation,[85] no evidence has shown that such decomposition undergoes in the homogenous water oxidation. It is important for developing highly active water oxidation catalysts to unveil what the true catalyst is when degradable catalytic complexes are employed as a catalyst.

We report herein the photocatalytic water oxidation using $[Ru(bpy)_3]^{2+}$ as a photosensitizer and $Na_2S_2O_8$ as a sacrificial electron acceptor in the presence of a water-soluble mononuclear cobalt complex with an organic ligand, $[Co^{II}(Me_6tren)(OH_2)]^{2+}$ (**1**), $[Co^{III}Cp^*(bpy)(OH_2)]^{2+}$ (**2**), $[Co^{II}(12\text{-TMC})]^{2+}$ (**3**) or $[Co^{II}(13\text{-TMC})]^{2+}$ (**4**) (12-TMC = 1,4,7,10-tetramethyl-1,4,7,10-tetraazacyclododecane and 13-TMC = 1,4,7,10-tetramethyl-1,4,7,10-tetraazacyclotridecane) (Chart 1). The catalytic reactivity in water oxidation using **1**–**4** as precatalysts was compared with that using $Co(NO_3)_2$ possessing no organic ligands but reported to catalyse water oxidation.[77–80] The kinetic analysis and the characterization of the actual reactive catalyst together with oxidation of the ligands have revealed that both **1** and **2** were converted to nanoparticles during the photocatalytic water oxidation and that the nanoparticles composed of $Co(OH)_x$ are the active catalysts for the water oxidation reactions.

2. Experimental section

All chemicals commercially available were used without further purification unless otherwise noted. $Co(NO_3)_2$ and 2,2′-bipyridine were purchased from Wako Pure Chemical Industries Ltd. Pentamethylcyclopentadiene was obtained from Kanto Chemical Co., Inc. $[Ru(bpy)_3]Cl_2$ was obtained from Tokyo Chemical Industry Co., Ltd. $Co(ClO_4)_2$ and tris(2-ethylamino)amine were supplied from Sigma-Aldrich Co. Purified water (18.2 MΩ cm) was obtained using a Milli-Q system (Millipore, Direct-Q 3 UV). $[Ru(bpy)_3](ClO_4)_2$ was synthesized by adding an aqueous solution of $HClO_4$ to an aqueous solution of $[Ru(bpy)_3]Cl_2$. $[Co^{II}(Me_6tren)(OH_2)](ClO_4)_2$ (**1**),[87–89] $[Co^{III}(Cp^*)(bpy)(OH_2)](PF_6)_2$ (**2**)[90,91] and $[Ru(bpy)_3](ClO_4)_3$[78] were synthesized according to literature procedures and characterized by electrospray ionization mass spectroscopy and ^1H NMR (see ESI†). Authentic Co_3O_4 was synthesized according to previous reports.[92,93] $[Co^{II}(12\text{-TMC})](ClO_4)_2$ and $[Co^{II}(13\text{-TMC})](ClO_4)_2$ were synthesized according to a previous report.[94]

2.1. Photocatalytic water oxidation

Photocatalytic water oxidation was performed as follows. A cobalt complex or $Co(NO_3)_2$ (0.0050–2.5 mM) was added to a buffer solution (50 mM, pH 7.0 and 8.0 for phosphate buffer and 100 mM, pH 9.0 and 10 for borate buffer) containing $Na_2S_2O_8$ (10 or 50 mM) and $[Ru(bpy)_3](ClO_4)_2$ (0.50 mM)

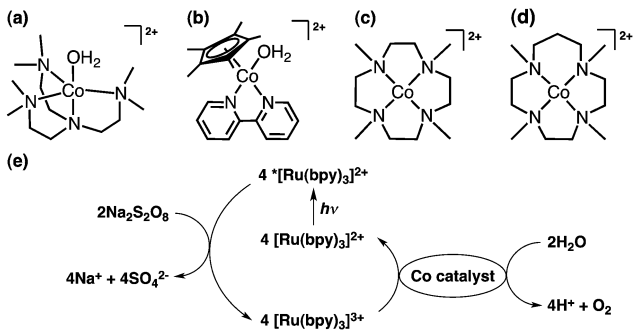

Chart 1 Chemical structures of mononuclear water-soluble cobalt complexes used as precatalysts: (a) $[Co^{II}(Me_6tren)(OH_2)]^{2+}$ (**1**), (b) $[Co^{III}(Cp^*)(bpy)(OH_2)]^{2+}$ (**2**), (c) $[Co^{II}(12\text{-TMC})]^{2+}$ (**3**) and (d) $[Co^{II}(13\text{-TMC})]^{2+}$ (**4**). (e) A scheme showing the overall catalytic cycle for photocatalytic water oxidation by $[Ru(bpy)_3]^{2+}$, $Na_2S_2O_8$ and a cobalt-containing catalyst.

purged with Ar gas for 10 min in a vial (i.d. ~2 cm) sealed with a rubber septum. The reactions were started by irradiating the solution with a Xe lamp (500 W) through a transmitting glass filter ($\lambda > 420$ nm) at room temperature. After each irradiation time, 100 μL of Ar was injected into the vial and then the same volume of gas in the headspace of the vial was sampled by a gas tight syringe and used for gas chromatography (GC) analysis. The O_2 in the sampled gas was separated by passing through a molecular sieve 5A column with an Ar carrier gas and quantified by a Thermal Conductivity Detector (TCD) (Shimadzu GC-17A). The total amount of evolved O_2 was calculated from the concentration of O_2 in the headspace gas.

Water oxidation with $[Ru(bpy)_3]^{3+}$ was performed as follows. A buffer solution (pH 8.0) containing a Co species (50 μM) in a vial sealed with a rubber septum was carefully deaerated by Ar gas for 10 min. The solution was withdrawn (2.0 mL) by a syringe and injected into 3.0 μmol (1.5 mM) of $[Ru(bpy)_3]^{3+}$ in another vial sealed with a rubber septum with flowing Ar gas. After the solution was injected completely and Ar gas was stopped, the solution was stirred vigorously for 10 min. A small portion (100 μL) of the gas in the headspace of the vial was sampled by a gas-tight syringe and used for gas analysis by GC.

The quantum yields of O_2 evolution were determined for the photocatalytic water oxidation under the following conditions. A square quartz cuvette (light path length: 10 mm), which was filled with a buffer solution (50 mM, pH 8.0 phosphate buffer) containing $Na_2S_2O_8$ (10 mM), $[Ru(bpy)_3](ClO_4)_2$ (0.50 mM) and **1** or **2** (50 μM), was irradiated with monochromatized light of $\lambda = 450 \pm 10$ nm from a Shimadzu RF-5300PC fluorescence spectrophotometer. The total number of incident photons was measured by a standard method using an actinometer (potassium ferrioxalate, $K_3[Fe^{III}(C_2O_4)_3]$) in an aqueous solution at room temperature where photon flux was determined to be 3.67×10^{-8} einstein s^{-1}. The evolved O_2 in a headspace of the cuvette was quantified by GC.

2.2. CO_2 detection

A buffer solution (pH 9.0, 2.0 mL) containing $Na_2S_2O_8$ (50 mM), $[Ru(bpy)_3](ClO_4)_2$ (0.50 mM) and cobalt catalysts (0–2.5 mM) was sealed in a vial with a rubber septum. The solution was carefully deaerated by bubbling N_2 gas for 10 min. After photoirradiation of the solution by a Xe lamp ($\lambda > 420$ nm), a small portion (50 μL) of the gas in the headspace was extracted by a gas-tight syringe and analysed by a Shimadzu GC-14B gas chromatograph (N_2 carrier, active carbon with a particle size of 60–80 mesh at 353 K) equipped with a TCD.

2.3. Spectroscopic measurements

^{1}H NMR spectra were recorded on a JEOL JNM-AL300 spectrometer in CD_3CN or D_2O solutions. Dynamic light scattering (DLS) measurements were performed with a Zetasizer Nano ZS instrument (Malvern Instruments Ltd., USA) for reaction solutions. The DLS instrument used in this study can detect the particle sizes ranging from 0.6 to 6000 nm. UV-vis absorption spectra were recorded on a Hewlett Packard 8453 diode array spectrophotometer.

2.4. Electrochemical measurements

Cyclic voltammetry (CV) was performed on an ALS 630B electrochemical analyser using a glassy carbon electrode as a working electrode, a saturated calomel electrode (SCE) as a reference electrode, and a Pt wire as an auxiliary electrode. Cyclic voltammograms were obtained in buffer solutions (pH 8.0, 2.0 mL) containing ligands (4.0 mM) at room temperature with a scanning rate of 100 mV s^{-1}.

2.5. Characterization of particles

Transmission electron microscope (TEM) images of nanoparticles, which were mounted on a copper microgrid coated with elastic carbon, were observed by a JEOL JEM-2100 operating at 200 keV. X-ray photoelectron spectra (XPS) were measured by a Kratos Axis 165x with a 165 mm hemispherical electron energy analyser. The incident radiation was Mg $K\alpha$ X-ray (1253.6 eV) at 200 W and a charge neutralizer was turned on for acquisition. Each sample was attached to a stainless stage with a double-sided carbon Scotch tape. The binding energy of each element was corrected by C 1s peak (284.6 eV) from residual carbon. TG/DTA data were recorded on an SII TG/DTA 7200 instrument. Each sample was heated from 25 °C to 100 °C (held at 100 °C for 10 min) and from 100 °C to 300 °C with a ramp rate of 2 °C min^{-1}. A certain amount of α-Al_2O_3 was used as a reference for DTA measurements. Powder X-ray diffraction (XRD) patterns were recorded by a Rigaku Ultima IV. Incident X-ray radiation was produced by Cu X-ray tube, operating at 40 kV and 40 mA with Cu $K\alpha$ radiation of 1.54 Å. The scanning rate was 4° per min from 10° to 80° in 2θ.

3. Results and discussion

3.1. Photocatalytic water oxidation with cobalt complexes as precatalysts

The reaction was executed by photoirradiation ($\lambda > 420$ nm) of a buffer solution (2.0 mL, initial pH 8.0) containing 0.50 mM $[Ru(bpy)_3]^{2+}$, 10 mM $Na_2S_2O_8$ and a cobalt complex, $[Co^{II}(Me_6tren)(OH_2)]^{2+}$ (**1**), $[Co^{III}(Cp^*)(bpy)(OH_2)]^{2+}$ (**2**), $[Co^{II}(12\text{-TMC})]^{2+}$ (**3**) or $[Co^{II}(13\text{-TMC})]^{2+}$ (**4**) (see Chart 1), or $Co(NO_3)_2$ (50 μM) as a precatalyst. The time courses of O_2 evolution in the headspace of a vial are shown in Fig. 1. No O_2 evolution was confirmed from a reaction solution without cobalt species. O_2 evolution was observed with all cobalt species, indicating cobalt species are an effective precatalyst for the photocatalytic water oxidation. As previously reported, $Na_2S_2O_8$ acts as a two-electron acceptor (eqn (1)).[83]

$$2H_2O + 2Na_2S_2O_8 \rightarrow O_2 + 4H^+ + 4Na^+ + 4SO_4^{2-} \quad (1)$$

In such a case, the stoichiometric amount of O_2 evolution should be 10 μmol in the present reaction system. Among the reaction systems with Co species, the largest amount of evolved O_2 was obtained with precatalyst **1** (5.4 μmol), where the amount of evolved O_2 increases in the order of **1** ≈ $Co(NO_3)_2$ > **3** > **2** > **4**.

Table 1 summarizes the turnover numbers (TONs) in 10 min based on Co in a solution and O_2 yields of the reaction systems containing cobalt complexes **1**–**4** as precatalysts in the

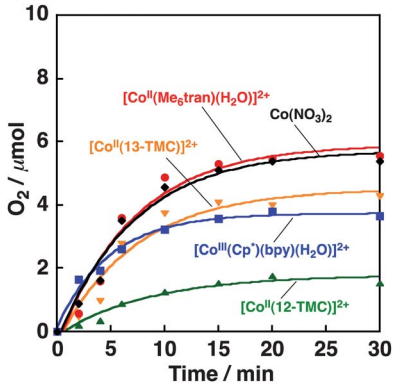

Fig. 1 Time courses of O_2 evolution under photoirradiation (Xe lamp, $\lambda > 420$ nm) of a buffer solution (2.0 mL, 50 mM phosphate, pH 8.0) containing $[Ru(bpy)_3]^{2+}$ (0.50 mM), $Na_2S_2O_8$ (10 mM) and a mononuclear cobalt complex (50 μM), $[Co^{II}(Me_6tren)(OH_2)]^{2+}$ (red), $[Co^{III}(Cp^*)(bpy)(OH_2)]^{2+}$ (blue), $[Co^{II}(12\text{-}TMC)]^{2+}$ (green), $[Co^{II}(13\text{-}TMC)]^{2+}$ (yellow) or $Co(NO_3)_2$ (50 μM, black) as a precatalyst.

photocatalytic water oxidation together with those of $Co(NO_3)_2$ and cobalt complexes reported in the literature.[83,86] The direct comparison of catalytic activity reported in the literature is difficult, because catalytic behaviour highly depends on a trivial change in reaction conditions. Additionally, coexisting ions such as counter anions influenced the catalytic behaviour of Co species. When $[Ru(bpy)_3]Cl_2$ was employed as a photosensitizer instead of $[Ru(bpy)_3](ClO_4)_2$, the O_2 yield was suddenly decreased from 54% to only 9% in the water oxidation with precatalyst **1** (Fig. S1 in ESI†). However, the TON of 54 obtained with precatalyst **1** is similar to those of $Co(NO_3)_2$ and $[Co^{II}_4(H_2O)_2(PW_9O_{34})_2]^{10-}$.[83] The TON of 29 obtained with precatalyst **2** is higher than that of $[Co^{III}_4O_4(OAc)_4(py)_4]$ (TON: 10).[86]

The reaction mechanism in the photocatalytic water oxidation depicted in Chart 1e was evidenced by the two independent experiments, which confirmed the generation of $[Ru(bpy)_3]^{3+}$ by photoirradiation of the solution containing $[Ru(bpy)_3]^{2+}$ and $Na_2S_2O_8$ and the thermal water oxidation by $[Ru(bpy)_3]^{3+}$ in the presence of precatalyst **1** or **2**. Among the Co complexes of **1–4**, only complex **2** contains Co(III) species, which allows us to observe the ^1H NMR spectra of the ligands owing to the diamagnetic property of Co(III). Thus, we examined the photocatalytic water oxidation in detail with precatalyst **1** exhibiting the highest activity, precatalyst **2** containing Co(III) species and $Co(NO_3)_2$ possessing no organic ligand. As shown in Chart 1e and eqn (2), photoexcitation of $[Ru(bpy)_3]^{2+}$ results in generation of $[Ru(bpy)_3]^{3+}$ by the oxidative quenching of the photoexcited state ($^*[Ru(bpy)_3]^{2+}$: * denotes the excited state) with $Na_2S_2O_8$.

$$2[Ru^{II}(bpy)_3]^{2+} + Na_2S_2O_8 \xrightarrow{h\nu} 2[Ru^{III}(bpy)_3]^{3+} + 2Na^+ + 2SO_4^{2-} \quad (2)$$

The generation of $[Ru(bpy)_3]^{3+}$ was monitored by the absorption band at 670 nm assigned to $[Ru(bpy)_3]^{3+}$. The time course of $[Ru(bpy)_3]^{3+}$ generation by photoirradiation in the presence of $Na_2S_2O_8$ is shown in Fig. S2 in the ESI.† The efficiency of $[Ru(bpy)_3]^{3+}$ generation calculated from the absorbance change was around 60% at pH 8.0. An efficiency lower than 100% may result from the low oxidation efficiency of $[Ru^{II}(bpy)_3]^{2+}$ by one electron reduced $Na_2S_2O_8$[95,96] or the ligand oxidation of $[Ru(bpy)_3]^{3+}$ (*vide infra*).

The thermal water oxidation by $[Ru(bpy)_3]^{3+}$ (1.5 mM) in eqn (3) was examined in the presence of precatalyst **1** or **2** (50 μM) in 2.0 mL of a phosphate buffer (pH 8.0).

$$4[Ru^{III}(bpy)_3]^{3+} + 2H_2O \rightarrow 4[Ru^{II}(bpy)_3]^{2+} + O_2 + 4H^+ \quad (3)$$

When a buffer solution of **1** or **2** was added to $[Ru(bpy)_3]^{3+}$ at room temperature, the colour of the solution changed from green to orange within 5 min. Evolved O_2 in the headspace was analysed and quantified by GC after 10 min for each reaction system, where the O_2 yields with precatalysts **1** and **2** were 52 ± 5% and 36 ± 5%, respectively. Thus, the thermal water oxidation by $[Ru(bpy)_3]^{3+}$ was achieved by precatalyst **1** or **2**. Isotope-labelling experiments using ^{18}O-enriched water (44.9%) instead of $H_2{}^{16}O$ were conducted with precatalyst **1**, indicating that evolved O_2 comes exclusively from water (Fig. S3 in ESI†). These experimental results support the stepwise process of the photocatalytic water oxidation depicted in Chart 1c.

The quantum yields for the photocatalytic water oxidation with precatalysts **1** and **2** at pH 8.0 were determined to be 32% and 30%, respectively (see Experimental section). These quantum yields were determined by dividing the net values for precatalysts **1** (19%) and **2** (18%) by the efficiency of $[Ru(bpy)_3]^{3+}$ generation (60% at pH 8.0) by photoirradiation in the presence of $Na_2S_2O_8$ (eqn (2)). The quantum yields normalized by the efficiency of $[Ru(bpy)_3]^{3+}$ generation were as high as that of $[Co^{II}_4(H_2O)_2(PW_9O_{34})_2]^{10-}$ (30%) at pH 8.0.[83] TONs, O_2 yields and quantum yields of precatalysts **1** and **2** in the photocatalytic water oxidation were similar to those of cobalt catalysts previously reported.[83,86]

Table 1 Turnover numbers (TONs) and O_2 yields for photocatalytic water oxidation with cobalt species (precatalysts) compared with reported TONs and O_2 yields under the condition of pH 8.0

Co species (precatalysts)	TON[a]	Yield[b] (%)	Ref.
1	54[c]	54 (62[d])	This work
2	29[c]	29 (60[d])	This work
3	16[c]	16	This work
4	41[c]	41	This work
$Co^{II}(NO_3)_2$	52[c]	52 (22[d])	This work
$[Co^{II}_4(H_2O)_2(PW_9O_{34})_2]^{10-}$	56[e]	45	83
$Co^{III}_4O_4(OAc)_4(py)_4$[f]	10[g]	31	86

[a] TON is defined as the total number of moles of O_2 per mole of precatalyst. [b] Yield is defined as twice the number of moles of O_2 per mole of $Na_2S_2O_8$. [c] Catalyst concentration was 50 μM. [d] At pH 10. [e] TON per one metal centre and concentration of catalysts was 5.0 μM. [f] OAc = acetate, py = pyridine. [g] TON per one metal centre and at pH 7.

3.2. Effect of pH on photocatalytic water oxidation

The photocatalytic water oxidation was examined under various pH conditions ranging from 6.0 to 10.0. High pH is thermodynamically favourable for the water oxidation. However, a spontaneous reduction of $[Ru(bpy)_3]^{3+}$ to $[Ru(bpy)_3]^{2+}$ accompanied with the oxidation of bpy ligand has also been reported at high

pH, leading to degradation of the photosensitizer.[78,79] In order to investigate the effect of pH on the O_2 yield of the photocatalytic water oxidation in the presence of **1**, **2** or $Co(NO_3)_2$ as a pre-catalyst, the initial pH of the reaction solution was set to be between 6.0 and 10 by employing two buffers, phosphate buffer (pH 6.0–8.0) and borate buffer (pH 9.0–10). Fig. 2 shows the time courses of O_2 evolution by photoirradiation ($\lambda > 420$ nm) of a buffer solution (2.0 mL) containing $[Ru(bpy)_3]^{2+}$ (0.50 mM), $Na_2S_2O_8$ (10 mM) and precatalyst **1**, **2** or $Co(NO_3)_2$ (50 μM) under various pH conditions. The O_2 yield monotonously increased with increasing pH from 6.0 to 9.0 in the presence of precatalyst **1**. The O_2 yield obtained under the condition of pH 10 (61%) was comparable to that obtained under the condition of pH 9.0 (62%). Similarly, the higher O_2 yield was obtained at higher pH in the presence of precatalyst **2**. The catalytic activity observed with precatalyst **2** was low compared to that with precatalyst **1** under the condition of pH 8.0. However, the difference in the catalytic activity became smaller at pH 9.0. The O_2 yield increased under the conditions of higher pH, although O_2 evolution ceased within 15 min of photoirradiation at any pH.

When the photocatalytic water oxidation was conducted with $Co(NO_3)_2$ as a precatalyst under various pH conditions, the O_2 yield reached the maximum value of 52% at pH 8.0 and dramatically decreased to 22% at pH 10 as shown in Fig. 2c. This pH-dependent catalytic behaviour of $Co(NO_3)_2$ under the conditions of pH higher than 9.0 exhibits sharp contrast to the catalytic behaviour observed for precatalysts **1** and **2** where they maintained high catalytic reactivity under the conditions of pH higher than 9.0.

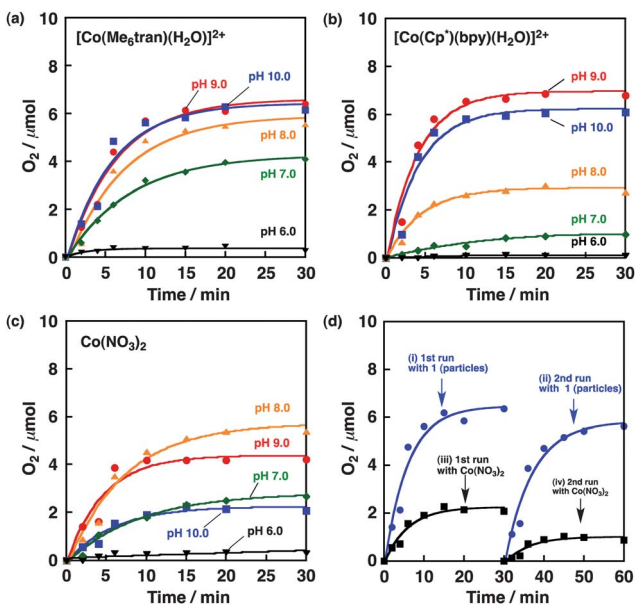

Fig. 2 Time courses of O_2 evolution under photoirradiation (Xe lamp, $\lambda > 420$ nm) of a buffer solution (2.0 mL) containing $[Ru(bpy)_3]^{2+}$ (0.50 mM) and $Na_2S_2O_8$ (10 mM) with a precatalyst (a) $[Co^{II}(Me_6\text{-tren})(OH_2)]^{2+}$ (**1**, 50 μM), (b) $[Co^{III}(Cp^*)(bpy)(OH_2)]^{2+}$ (**2**, 50 μM) or (c) $Co(NO_3)_2$ at an initial pH value of 6.0 (black triangle), 7.0 (green diamond), 8.0 (yellow triangle), 9.0 (red cycle) or 10 (blue square). (d) Time courses of O_2 evolution under photoirradiation (Xe lamp, $\lambda > 420$ nm) of a buffer solution (pH 10, 2.0 mL) containing $[Ru(bpy)_3]^{2+}$ (0.50 mM) and $Na_2S_2O_8$ (10 mM) with a precatalyst (i and ii) **1** (50 μM) and (iii and iv) $Co(NO_3)_2$ (50 μM). 2nd runs were performed by adding $Na_2S_2O_8$ (5.0 μmol) to the solutions after the 1st run.

The robustness of the reaction system with precatalyst **1** in comparison with that with $Co(NO_3)_2$ was examined by the further addition of $Na_2S_2O_8$, which is the sacrificial electron acceptor, to the solution after reactions at pH 10. The catalytic activity of $Co(NO_3)_2$ becomes maximum at pH 8.0. However, the decrease of pH to 6–7 after 1st run precluded the repeated examination (Fig. S4 in ESI†, pH 8.0). When $Na_2S_2O_8$ (5.0 μmol) was added to the solutions after the reactions at pH 10 for 30 min, successive O_2 evolution was observed from both solutions with precatalysts **1** and $Co(NO_3)_2$ as shown in Fig. 2d. However, the O_2 yield of the reaction with $Co(NO_3)_2$ in the 2nd run was only 10%, which is significantly lower than the O_2 yield of 22% in the 1st run, whereas the O_2 yield of the reaction with precatalyst **1** in the 2nd run was 54%, which is similar to that of the 1st run (61%). In the reaction solution used for the 2nd run, the concentration of $[Ru(bpy)_3]^{2+}$ and pH of the solution decreased to ~0.4 mM and ~9.5, respectively. However, these changes do not affect the catalytic behaviour significantly (Fig. 2).[97] These results clearly indicate that the reaction system with precatalyst **1** is more durable than that with $Co(NO_3)_2$. The robustness of the reaction system with precatalyst **1** can be ascribed to the presence of organic residues (*vide infra*).

3.3. Concentration effect of cobalt complexes on photocatalytic water oxidation

The concentration effect of precatalysts **1** and **2** on the O_2 yields at pH 9.0 was compared with $Co(NO_3)_2$. The time courses of O_2 evolution with different concentrations of the cobalt complexes and $Co(NO_3)_2$ are shown in Fig. 3, where O_2 evolved even when the concentration of cobalt species was as low as 5.0 μM. The maximum TON values based on Co were 420 for the reaction system with precatalyst **1**, 320 for that with precatalyst **2** and 315 for that with $Co(NO_3)_2$ at the concentration of 5.0 μM, indicating that **1** provides the most efficient catalyst for the photocatalytic water oxidation. These TON values were much higher than those at pH 8.0 with a high concentration of Co species (50 μM) (Table 1). The amount of evolved O_2 increased with an increase of the concentration of precatalyst **1** up to 50 μM with maximum O_2 yield of 62% (Fig. 3a). The O_2 yield was gradually decreased by a further increase in concentration of precatalyst **1**. When the concentration of precatalyst **1** was increased to 2.5 mM, no O_2 evolution was observed even at the initial stage of photoirradiation. As compared with precatalyst **1**, a similar trend of O_2 evolution was observed with precatalyst **2** (Fig. 3b). The O_2 yield reached a highest value of 65% when the concentration of precatalyst **2** was 50 μM. On the other hand, the O_2 yield gradually increased with an increase in concentration of $Co(NO_3)_2$, as shown in Fig. 3c. The highest O_2 yield with $Co(NO_3)_2$ was obtained at concentrations of 0.50 and 2.5 mM. The O_2 evolution ceased within 15 min from the reaction solution with precatalyst **1**, **2** or $Co(NO_3)_2$ at any concentrations because of degradation of bpy ligand of $[Ru(bpy)_3]^{2+}$ under the present reaction conditions (*vide infra*).

The concentration effects of precatalysts **1** and **2** compared with $Co(NO_3)_2$ on the O_2 evolution at pH 9.0 are summarized in Fig. 3d, where the O_2 yields of the photocatalytic water oxidation

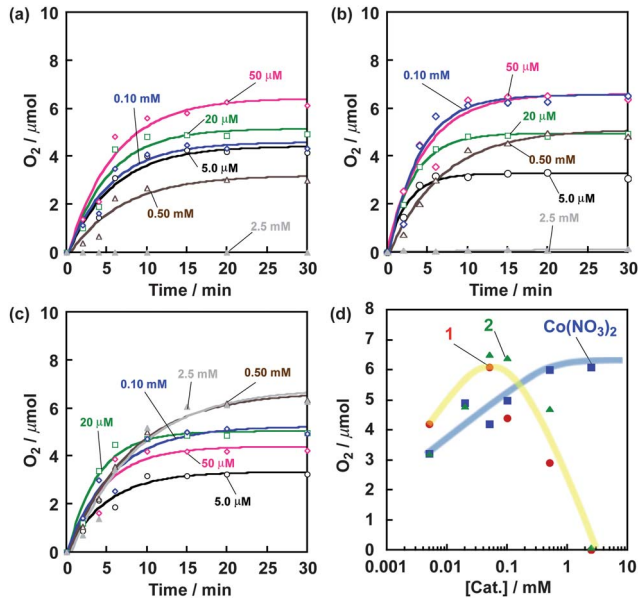

Fig. 3 Time courses of O_2 evolution under irradiation with visible light (Xe lamp, $\lambda > 420$ nm) at different concentrations of precatalyst (a) **1**, (b) **2** and (c) $Co(NO_3)_2$ [5.0 μM (black circle), 20 μM (green square), 50 μM (pink diamond) and 0.10 mM (blue diamond), 0.50 mM (blown triangle) and 2.5 mM (grey triangle)] in the solution containing $[Ru(bpy)_3]^{2+}$ (0.50 mM) and $Na_2S_2O_8$ (10 mM) in 2.0 mL of borate buffer (100 mM, pH 9.0). (d) Dependence of O_2 evolution on concentrations of precatalysts, **1** (red circles), **2** (green triangles) and $Co(NO_3)_2$ (blue square) after 20 min photoirradiation (Xe lamp, $\lambda > 420$ nm) of the solution (pH 9.0).

by photoirradiation of a buffer solution (pH 9.0) containing $[Ru(bpy)_3]^{2+}$, $Na_2S_2O_8$ and various concentrations of precatalysts **1** (red circles), **2** (green triangles) and $Co(NO_3)_2$ (blue squares) are shown. In the presence of $Co(NO_3)_2$, the O_2 yield increased with an increase in concentration of $Co(NO_3)_2$ up to 0.50 mM. The highest O_2 yield obtained with 0.50 mM of $Co(NO_3)_2$ was maintained with a higher concentration (2.5 mM) of $Co(NO_3)_2$. On the other hand, a peculiar behaviour of O_2 yields was observed depending on concentrations of precatalysts **1** and **2**. The O_2 yields were the highest when the concentration of precatalysts **1** and **2** was around 50 μM, and then decreased with an increase in concentrations of precatalysts **1** and **2**. Finally, no O_2 evolution was observed when the concentrations of precatalysts **1** and **2** were 2.5 mM. These results indicate that cobalt complexes **1** and **2** were converted to different species at concentrations >2.5 mM. Actually, formation of precipitates/particles in the solution was observed after photocatalytic water oxidation with 2.5 mM of precatalyst **1**.

3.4. Photocatalytic water oxidation by particles derived from complex 1

The particles/precipitates were used to examine the activity in photocatalytic water oxidation to confirm that the particles are indeed the actual catalysts for the photocatalytic water oxidation. As shown in Fig. 4a, no O_2 was evolved with complex **1** (2.5 mM) in the buffer solution containing $Na_2S_2O_8$ and $[Ru(bpy)_3]^{2+}$ under photoirradiation (1st run). The reason for no

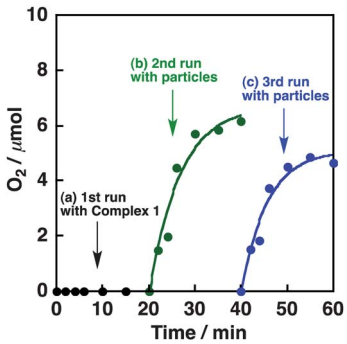

Fig. 4 Time courses of O_2 evolution under photoirradiation (Xe lamp, $\lambda > 420$ nm) of a buffer solution (2.0 mL, 100 mM borate, pH 9.0) containing $[Ru(bpy)_3]^{2+}$ (0.50 mM) and $Na_2S_2O_8$ (10 mM) (a) with complex **1** (2.5 mM) (1st run), (b) with nanoparticles (~0.12 mg) derived from **1** in a fresh solution (2nd run) and (c) with the nanoparticles collected after 2nd run with another fresh solution (3rd run).

O_2 evolution at the 1st run may be that the oxidation of the organic ligands of **1** proceeds prior to water oxidation. Particles formed at the 1st run were separated from the reaction solution by centrifugation, washed with water and ethanol successively and dried *in vacuo* at room temperature.

When the particles (~0.12 mg) were employed as a catalyst at the 2nd run, efficient O_2 evolution (yield: 61%) was observed as shown in Fig. 4b. The yield obtained with the particles was as high as that obtained with a low concentration of precatalyst **1** (50 μM) as shown in Fig. 3. The robustness of the collected nanoparticles was confirmed by using them in a further reaction cycle. A slightly lower but significant amount of O_2 evolution (yield: 47%) was obtained in the 3rd run with the particles collected from the reaction solution of the 2nd run as shown in Fig. 4c. The lower O_2 yield in the 3rd run was due to the recovery loss of catalytic particles. These results clearly demonstrated that the actual catalyst for the photocatalytic water oxidation was the particles derived from **1**. Thus, the transformation of **1** and **2** into true catalysts during the photocatalytic water oxidation were investigated in detail by ^{1}H NMR measurements (*vide infra*).

3.5. Oxidative decomposition of cobalt complexes

Fig. 5 shows the ^{1}H NMR spectra of complex **2** (1.0 mM) in a buffer solution (D_2O, pD 10) containing $[Ru(bpy)_3](ClO_4)_2$ (0.20 mM) and $Na_2S_2O_8$ (10 mM). The lower magnetic fields of the NMR spectra are magnified in Fig. S5 in the ESI.† Before photoirradiation, two sets of bpy ligands of **2** (black circles) and $[Ru(bpy)_3]^{2+}$ (pink triangles) were observed in the lower magnetic field (7–10 ppm), and only one sharp peak appeared at 1.3 ppm assigned to methyl groups of Cp^* as shown in Fig. 5a. When the solution was photoirradiated for 30 min, the NMR peak assigned to the Cp^* ligand of **2** diminished, and small peaks in the range of 1–2.5 ppm and four peaks, which are in the range of 7–9 ppm, assigned to free bpy, appeared (Fig. 5b). This NMR spectral change suggested oxidative decomposition of the Cp^* ligand and dissociation of the bpy ligand from the cobalt ion or the oxidation of the cobalt ion from Co(III) to Co(IV). In order to confirm the possibility of cobalt ion oxidation, a reducing reagent of dihydronicotineamide adenine dinucleotide (NADH) was added

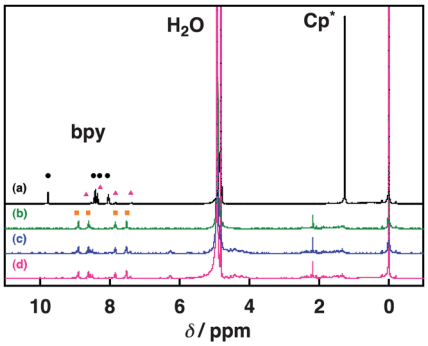

Fig. 5 ^{1}H NMR spectra of (a) **2** (2.0 mM) with $[Ru(bpy)_3]^{2+}$ (0.20 mM) and $Na_2S_2O_8$ (10 mM), (b) after photoirradiation of the aqueous solution for 30 min, (c) adding 1.0 mM of NADH to the photoirradiated solution and (d) solution containing NADH exposed to air for 1 h (black circles, bpy of **2**; pink triangles, bpy from $[Ru(bpy)_3]^{2+}$; yellow squares, free bpy) in a D_2O borate buffer (pD 10). Lower magnetic fields of the spectra are magnified in Fig. S5 in ESI.†

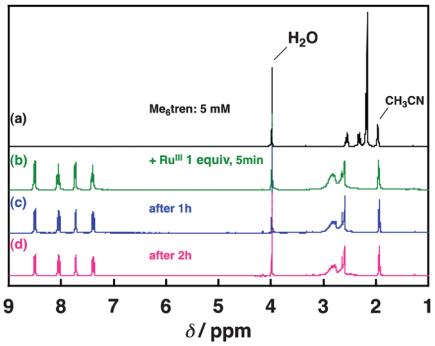

Fig. 6 ^{1}H NMR spectra of (a) Me_6tren (5.0 mM) and Me_6tren (5.0 mM) after reaction with $[Ru(bpy)_3]^{3+}$ (5.0 mM) for (b) 5 min, (c) 1 h and (d) 2 h in CD_3CN at 298 K.

to the solution after photoirradiation to reduce Co(IV) species, which might be formed during the photocatalytic oxidation. As shown in Fig. 5c, no significant change in the NMR spectrum was observed. Additionally, the solution was exposed to air to oxidize Co(II) species, which might be formed by over-reduction of Co(IV) species. However, no NMR spectral change was observed as shown in Fig. 5d. Thus, the spectral change caused by photoirradiation resulted from the oxidation of Cp^* ligand and dissociation of bpy ligand from the cobalt ion. The oxidation of the Cp^* ligand has been reported previously for the $[Ir(Cp^*)(H_2O)_3]^{2+}$ complex during water oxidation by cerium ammonium nitrate.[73] During the reaction, Cp^* was oxidized to acetic acid and formic acid. A similar oxidation may occur on the Cp^* ligand of **2** during the water oxidation by $[Ru(bpy)_3]^{3+}$.

Because **1** contains a paramagnetic Co(II) ion, ^{1}H NMR measurements were performed on the ligand of **1** (Me_6tren, 5.0 mM) in CD_3CN solution after oxidation with $[Ru(bpy)_3]^{3+}$ (5.0 mM) to examine the ligand oxidation. Fig. 6a indicates the reference spectrum of the solution without $[Ru(bpy)_3]^{3+}$, where ^{1}H NMR signals from methyl and methylene groups of Me_6tren appeared at 2.3 and 2.8 and 3.2 ppm. When 1 equiv. of $[Ru(bpy)_3]^{3+}$ was added to the solution, these NMR peaks became broadened and shifted to the lower magnetic field (2.5–3.0 ppm). The new peaks that appeared in the region of 7–9 ppm were assigned to $[Ru(bpy)_3]^{2+}$ and no peaks assigned to free bpy ligand were observed. No significant spectral change was observed after 1 or 2 h of the addition of $[Ru(bpy)_3]^{3+}$ to the solution at room temperature as shown in Fig. 6c and d, respectively. The ^{1}H NMR spectral change indicates that the oxidation of Me_6tren with $[Ru(bpy)_3]^{3+}$ readily occurred in CD_3CN. These results suggest that the ligand of **1** is oxidized during the photocatalytic water oxidation.

The electrochemical oxidation of the organic ligands of complexes **1–4** was performed to compare the reactivity of the ligands. Fig. 7 shows the cyclic voltammograms of the ligands (4.0 mM) in a pH 8.0 buffer solution. The anodic current with Me_6tren ligand of **1** started growing around 0.36 V *vs.* saturated calomel electrode (SCE) and reached more than 300 μA at 1.2 V as compared with the smaller anodic currents observed for Cp^*H (~50 μA), 12-TMC and 13-TMC (~180 μA), with which precatalyst **2–4** were less active than precatalyst **1** in photocatalytic water oxidation. Almost no anodic current was observed for the bpy ligand, while the bpy ligand easily dissociated from complex **2** during the photocatalytic water oxidation (Fig. 5). The oxidation of 12-TMC is similar to that of 13-TMC, however, the coordination length of 13-TMC to cobalt ion (Co–N) is longer than that of 12-TMC.[94] The weaker coordination of 13-TMC to cobalt ion may result in easy dissociation of 13-TMC from complex **4** as compared with that of 12-TMC. These results indicate that the ligand oxidation and dissociation from complexes result in the susceptibilities of the cobalt complexes to decomposition. Thus, the easier oxidation of Me_6tren ligand is most likely to lead to the higher activity of the formed nanoparticles. Additionally, the oxidation of the organic ligands of complexes **1–4** by $[Ru^{III}(bpy)_3]^{3+}$ in a CH_3CN solution was examined as shown in Fig. S6 in ESI,† where the Me_6tren, Cp*H, 12-TMC and 13-TMC ligands exhibited much larger reactivity than the bpy ligand in CH_3CN. The bpy ligand was also gradually oxidized by $[Ru^{III}(bpy)_3]^{3+}$ at a prolonged reaction time. The ligand oxidation by $[Ru^{III}(bpy)_3]^{3+}$ also matched the order of reactivity in photocatalytic water oxidation. The final products of the ligand oxidation during the photocatalytic water oxidation were examined in more detail (*vide infra*).

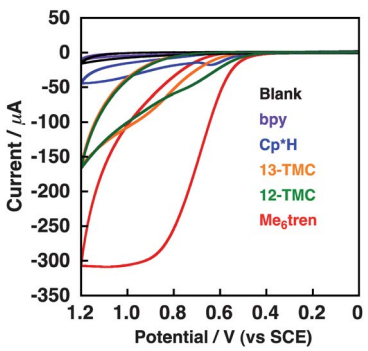

Fig. 7 Cyclic voltammograms of a buffer solution (pH 8.0, 50 mM; black line) containing ligands of **1–4** (4.0 mM); bpy (purple line), Cp*H (blue line), 13-TMC (yellow line), 12-TMC (green line) and Me_6tren (red line) at a scan rate of 100 mV s^{-1}.

3.6. CO_2 formation with high concentration of $Na_2S_2O_8$

The complete oxidation of Me_6tren provides water, NO_x and CO_2 as products. Among them, CO_2 can be easily detected and quantified by gas chromatography. The photocatalytic water oxidation was performed with a high concentration of $Na_2S_2O_8$ to fully oxidize the ligand. Fig. 8 shows the time courses of CO_2 formation by the photoirradiation of a buffer solution (pH 9.0) containing $Na_2S_2O_8$ (50 mM), $[Ru(bpy)_3]^{2+}$ (0.50 mM) and various concentrations of precatalyst **1** or $Co(NO_3)_2$ (0–2.5 mM). Even without precatalysts **1** and $Co(NO_3)_2$, CO_2 formation was observed after 20 min of the photoirradiation, because the ligand of $[Ru(bpy)_3]^{2+}$ was oxidized to CO_2 after 20 min in the reaction solution (Fig. 8a). The rapid degradation of $[Ru(bpy)_3]^{2+}$ can explain the cessation of the O_2 evolution in 15 min as observed in all the experiments in Fig. 1 and 2. The photoirradiation of a buffer solution containing $Na_2S_2O_8$ and $[Ru(bpy)_3]^{2+}$ for 2 h led to the evolution of 3.2 μmol of CO_2 (Fig. 8a). If all bpy ligands of $[Ru(bpy)_3]^{2+}$ in the solution was oxidized to CO_2, 30 μmol of CO_2 should be formed. The amount of 3.2 μmol of CO_2 corresponds to 11%, indicating that not all the bpy ligands were fully oxidized under the current reaction conditions. In the presence of $Co(NO_3)_2$ (0.05 mM) in the reaction solution, 8.4 μmol of CO_2 (28%) was formed (Fig. 8a), indicating that cobalt species act as a catalyst for the complete oxidation of the bpy ligand. The increase in $Co(NO_3)_2$ concentration from 0.050 mM to 2.5 mM resulted in an increase in O_2 evolution as shown in Fig. 3.

The presence of precatalyst **1** (0.050 mM) in place of $Co(NO_3)_2$ also resulted in an increase in the amount of evolved CO_2 (7.8 μmol) by photoirradiation for 2 h (Fig. 8b). CO_2 formation may be derived mainly from the bpy oxidation, because only 1.2 μmol of carbon atoms was included in Me_6tren ligand of **1** (0.050 mM). When the concentration of precatalyst **1** increased to 2.5 mM, precipitates were formed in the solution and no O_2 evolved but instead the largest amount of CO_2 evolution (10.9 μmol) was observed as shown in Fig. 8b. These results demonstrated that the ligand oxidation occurred prior to the water oxidation. The oxidation of the ligand resulted in the formation of Co cluster species, which are insoluble in water.

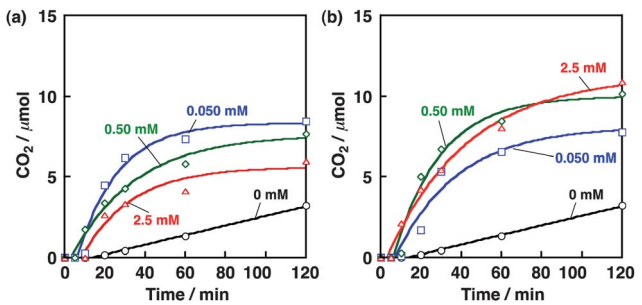

Fig. 8 Time courses of CO_2 evolution under photoirradiation (Xe lamp, $\lambda > 420$ nm) of a buffer solution (2.0 mL, 100 mM borate, pH 9.0) containing $[Ru(bpy)_3]^{2+}$ (0.50 mM), $Na_2S_2O_8$ (50 mM) and a cobalt precatalyst of (a) $Co(NO_3)_2$ or (b) **1** at concentrations of 0 mM (black circle), 0.050 mM (blue square), 0.50 mM (green diamond) and 2.5 mM (red triangle).

3.7. Characterization of nanoparticles formed from cobalt complexes by DLS, TEM, XPS and TG/DTA

In order to confirm formation of insoluble nanoparticles during the photocatalytic water oxidation, dynamic light scattering (DLS) measurements were conducted for aqueous solutions containing **1**, **2** or $Co(NO_3)_2$. When a buffer solution (pH 9.0) containing **1** (50 μM), $[Ru(bpy)_3]^{2+}$ (0.50 mM) and $Na_2S_2O_8$ (10 mM) was photoirradiated ($\lambda > 420$ nm) for 3 min, particles with an average size of 20 nm were detected as shown in Fig. 9a. The size distribution of the particles was 15–60 nm. No further significant change in the particle size was observed by prolonging the photoirradiation time to 30 min. In the reaction solution containing **2**, the size of formed particles ranged from 100 nm to 500 nm with photoirradiation for 3 min (black line) as shown in Fig. 9b. When the reaction time was prolonged to 10 min, the particle size became a little larger (blue broken line, 150 nm to 500 nm). However, the size became smaller (red dotted line, 80 nm to 200 nm) when the photoirradiation time was further prolonged to 30 min. The decrease in the size of nanoparticles resulted from a decrease in pH by generation of protons associated with the water oxidation (eqn. (1)), leading to the partial dissolution of the particles.

The size of particles derived from $Co(NO_3)_2$ (50 μM) increased to an average size of 500 nm from 50–100 nm by prolonging the photoirradiation time to 30 min as shown in Fig. 9c in contrast to the case of **2**. The size increase of particles leading to the decrease in the effective surface area can explain why the O_2 yield with $Co(NO_3)_2$ (50 μM) was lower as compared with **1** and **2** (Fig. 3). The formed particles were postulated as cobalt hydroxides, which formed due to the high pH. These results revealed that particles derived from **1**, **2** and $Co(NO_3)_2$ were formed even at the initial stage of the photoirradiation.

Judging from the results of ^{1}H NMR, DLS measurements and the ligand oxidation by $[Ru(bpy)_3]^{3+}$ described above, the decomposition of **1** and **2** resulted in the formation of nanoparticles as soon as the photocatalytic water oxidation was started. The particles formed after the photocatalytic water oxidation of a buffer solution (pH 9.0) containing $Na_2S_2O_8$ (10 mM), $[Ru(bpy)_3]^{2+}$ (0.50 mM) with **1**, **2** or $Co(NO_3)_2$ (2.5 mM) were separated from the reaction solution by centrifugation, washed with water several times and dried *in vacuo* at room temperature. The precipitates obtained were then analysed by transmission electron microscopy (TEM). TEM measurements were performed on the particles derived from **1**, **2** and $Co(NO_3)_2$.

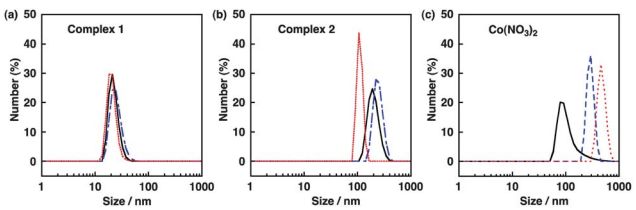

Fig. 9 Particles size and their distribution determined by DLS measurements of particles derived from (a) **1**, (b) **2** and (c) $Co(NO_3)_2$. Particles formed by photoirradiation (Xe lamp, $\lambda > 420$ nm) of a buffer solution (2.0 mL, 100 mM borate, pH 9.0) containing **1**, **2** or $Co(NO_3)_2$ (50 μM), $[Ru(bpy)_3]^{2+}$ (0.50 mM) and $Na_2S_2O_8$ (10 mM) for 3 min (black line), 10 min (blue broken line) and 30 min (red dotted line).

TEM images of the particles derived from **1** are displayed in Fig. 10a and b. From the low magnification image (Fig. 10a), the size of particles ranged from 10 to 50 nm, which is nearly identical to the particles sizes determined by DLS (15–60 nm). From a high magnification image of Fig. 10b, smaller particles of sizes of a few nanometres were also formed, indicating that the particles observed in Fig. 10a are secondary particles. Fig. 10c and d show the TEM images of nanoparticles derived from **2**. Judging from these images, the particles are composed of large needle-like-shaped particles and small spherical particles. The size determined for the particles derived from **2** by the DLS measurements ranged from 100 to 300 nm, which agreed with the length of needle-like particles. The size decrease after 30 min observed by DLS resulted from the dissociation of stacking needle-like particles. The TEM images of particles derived from $Co(NO_3)_2$ indicated that the size of primary particles is around 10 nm as shown in Fig. 10f. The particles aggregated to form secondary particles of sizes of 100 to 800 nm as shown in Fig. 10e and f. Thus, the sizes of secondary particles derived from **1**, **2** and $Co(NO_3)_2$ were quite consistent with those determined by DLS. Powder X-ray diffraction measurements were also performed on these particles. However, no peak was observed, suggesting that the particles are amorphous (Fig. S7 in ESI†).

In order to determine the surface conditions of the nanoparticles formed in the photocatalytic water oxidation with **1**, X-ray photoelectron spectroscopy (XPS) measurements of the nanoparticles were performed for the energy regions of Co 2p, O 1s, Ru 3d and C 1s, although no peak was observed in the Ru 3d region. Fig. 11a displays the XPS spectrum for Co 2p of the nanoparticles derived from **1** together with an authentic sample of Co_3O_4. Co $2p_{1/2}$ and Co $2p_{3/2}$ peaks of the nanoparticles appeared at 780.0 eV and 795.3 eV with weak satellite peaks. Similarly, Co_3O_4 shows two intense peaks at 779.8 eV for Co $2p_{3/2}$ and at 795.1 eV for Co $2p_{1/2}$ with weak satellite peaks. The presence of satellite peaks has been reported to support the presence of Co(II) species.[93,98,99] Slightly intense satellite peaks observed with the nanoparticles are ascribed to the higher ratio of Co(II) species compared with the authentic Co_3O_4 sample, because **1** exclusively contained Co(II) species before the photocatalytic water oxidation.

In Fig. 11b, the O 1s peak of the nanoparticles appeared at 531.5 eV, which is in a higher binding energy region compared

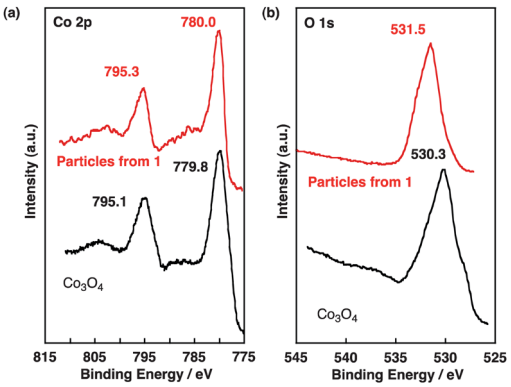

Fig. 11 X-ray photoelectron spectra of particles derived from **1** (red) and Co_3O_4 (black) as a reference compound in the energy regions of (a) Co 2p and (b) O 1s. The binding energy of each element was corrected by the C 1s peak (284.6 eV).

with the O 1s peak of Co_3O_4 (530.3 eV) by 1.2 eV. An increase in the binding energy of the O 1s peak of the nanoparticles has often been observed for metal hydroxide species.[93] Thus, it can be concluded that the surface of the nanoparticles derived from **1** under the photocatalytic water oxidation is mainly composed of $Co(OH)_x$, which can act as the actual catalyst for the photocatalytic water oxidation.

TG/DTA measurements have been preformed to confirm the occlusion of carbonaceous residues in the particles derived from **1**. Fig. 12 shows the TG/DTA curve of nanoparticles derived from **1** in which the TG curve can be divided into two consecutive stages with weight loss. The first step of weight loss around 110 °C corresponds to the removal of physisorbed water. The second step of the weight loss from 150 °C to 220 °C accompanied by an exothermic peak was assigned to oxidative removal of carbonaceous residues derived from the ligand, because precatalyst **1** thermally decomposes around 250 °C, which is a slightly higher temperature than the observed weight-loss temperature for nanoparticles derived from **1** as shown in Fig. S8a (ESI†). The steep weight loss observed in this step was *ca.* 14%. The results indicated that the carbonaceous residues occluded in **1** could prevent particles from aggregating and act as a modifier of catalytic particles. Thus, the easily oxidized ligand may be converted to carbonaceous residues, which can be

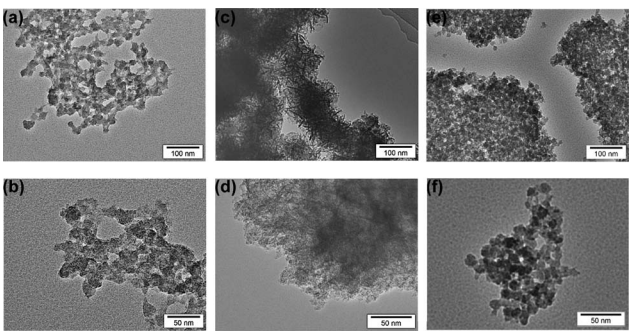

Fig. 10 TEM images of nanoparticles formed during the photocatalytic water oxidation with (a and b) **1**, (c and d) **2** and (e and f) $Co(NO_3)_2$ in a buffer solution (pH 9) containing $[Ru(bpy)_3]^{2+}$ (0.50 mM) and $Na_2S_2O_8$ (10 mM).

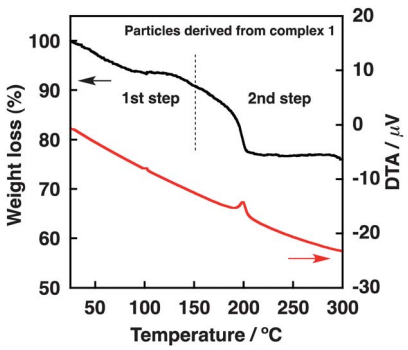

Fig. 12 TG/DTA data for nanoparticles derived from complex **1** (TG curve: black, DTA curve: red). The temperature increased from 25 °C to 300 °C with a ramp rate of 2 °C min^{-1}.

occluded in the nanoparticles. The carbonaceous residues prevent the aggregation of the nanoparticles during the photocatalytic water oxidation (Fig. 9). As compared to the Me_6tren ligand of **1**, it was more difficult to oxidize the ligand of **2** (Fig. 5). The carbonaceous residues were hardly formed on the surface of nanoparticles derived from **2**, because the stable ligands can dissociate from cobalt metal ions before the ligand oxidation. As shown in Fig. 5, free bpy ligands were released during the oxidation reaction.

Conclusions

O_2 evolution by the photocatalytic water oxidation was examined with $[Ru(bpy)_3]^{2+}$ as a photosensitizer and $Na_2S_2O_8$ as an electron acceptor in the presence of water-soluble cobalt complexes, $[Co^{II}(Me_6tren)(OH_2)]^{2+}$ (**1**), $[Co^{III}(Cp^*)(bpy)(OH_2)]^{2+}$ (**2**), $[Co^{II}(12\text{-TMC})]^{2+}$ (**3**), $[Co^{II}(13\text{-TMC})]^{2+}$ (**4**) and $Co(NO_3)_2$ as precatalysts to evolve O_2 with yields in the order of **1** ≈ $Co(NO_3)_2$ > **3** > **2** > **4**. Isotope labelling experiments with $H_2{}^{18}O$ clearly indicate that evolved O_2 derived from water. The O_2 yield in the photocatalytic water oxidation increased with increasing concentrations of precatalysts **1** and **2**, but dramatically decreased when the concentrations of the precatalysts were larger than 0.10 mM. CO_2 was evolved instead of O_2 with increase in $Na_2S_2O_8$ concentration. The observation of the CO_2 formation indicates that the organic ligand oxidation occurred during the photocatalytic water oxidation. Formation of nanoparticles by the decomposition of cobalt complexes was evidenced by the DLS and TEM measurements. The XPS measurements of the nanoparticle products suggest that the surface of the particles is composed of Co(II), Co(III) and OH species. Thus, the present results led us to conclude that the mononuclear cobalt complexes with organic ligands **1** and **2** act as efficient precatalysts, which are oxidized during the photocatalytic water oxidation to produce actual reactive catalysts, *i.e.*, nanoparticles composed of $Co(OH)_x$. Although the organic ligands would not be in their original forms in the catalytic particles, the carbonaceous residues derived from them act as a modifier or capping agent of the nanoparticles. Thus, the choice of the ligand of cobalt complexes is important to obtain an efficient and robust catalytic material for water oxidation.

Acknowledgements

This work at OU was supported by a Grant-in-Aid (No. 20108010), and a Global COE program, "the Global Education and Research Centre for Bio-Environmental Chemistry" from the Ministry of Education, Culture, Sports, Science and Technology, Japan. The work at EWU was supported by NRF/MEST of Korea through CRI, WCU (R31-2008-000-10010-0), GRL (2010-00353) Programs and the 2011 KRICT OASIS Project. We sincerely acknowledge Research Centre for Ultra-Precision Science & Technology for TEM measurements and Prof. Norimitsu Tohnai at OU for XRD measurements.

Notes and references

1 N. S. Lewis and D. G. Nocera, *Proc. Natl. Acad. Sci. U. S. A.*, 2006, **103**, 15729.
2 H. Dau and I. Zaharieva, *Acc. Chem. Res.*, 2009, **42**, 1861.
3 Y. Umena, K. Kawakami, J.-R. Shen and N. Kamiya, *Nature*, 2011, **473**, 55.
4 D. Gust, T. A. Moore and A. L. Moore, *Acc. Chem. Res.*, 2009, **42**, 1890.
5 P. E. M. Siegbahn, *Acc. Chem. Res.*, 2009, **42**, 1871.
6 A. Magnuson, M. Anderlund, O. Johansson, P. Lindblad, R. Lomoth, T. Polivka, S. Ott, K. Stensjo, S. Styring, V. Sundstrom and L. Hammarstrom, *Acc. Chem. Res.*, 2009, **42**, 1899.
7 S. Fukuzumi, Y. Yamada, T. Suenobu, K. Ohkubo and H. Kotani, *Energy Environ. Sci.*, 2011, **4**, 2754.
8 S. Fukuzumi, *Eur. J. Inorg. Chem.*, 2008, 1351.
9 M. W. Kanan, Y. Surendranath and D. G. Nocera, *Chem. Soc. Rev.*, 2009, **38**, 109.
10 D. G. Nocera, *Chem. Soc. Rev.*, 2009, **38**, 13.
11 S. Fukuzumi, *Bull. Chem. Soc. Jpn.*, 2006, **79**, 177.
12 S. Fukuzumi, *Phys. Chem. Chem. Phys.*, 2008, **10**, 2283.
13 K. Ohkubo and S. Fukuzumi, *Bull. Chem. Soc. Jpn.*, 2009, **82**, 303.
14 R. Eisenberg and H. B. Gray, *Inorg. Chem.*, 2008, **47**, 1697.
15 M. H. Huynh and T. J. Meyer, *Chem. Rev.*, 2007, **107**, 5004.
16 F. Jiao and H. Frei, *Energy Environ. Sci.*, 2010, **3**, 1018.
17 L. Duan, L. Tong, Y. Xu and L. Sun, *Energy Environ. Sci.*, 2011, **4**, 3296.
18 S. Romain, L. Vigara and A. Llobet, *Acc. Chem. Res.*, 2009, **42**, 1944.
19 X. Sala, I. Romero, M. Rodriguez, L. Escriche and A. Llobet, *Angew. Chem., Int. Ed.*, 2009, **48**, 2842.
20 T. A. Betley, Q. Wu, T. Van Voorhis and D. G. Nocera, *Inorg. Chem.*, 2008, **47**, 1849.
21 W. J. Youngblood, S. H. A. Lee, K. Maeda and T. E. Mallouk, *Acc. Chem. Res.*, 2009, **42**, 1966.
22 J. L. Cape and J. K. Hurst, *J. Am. Chem. Soc.*, 2008, **130**, 827.
23 R. Brimblecombe, G. F. Swiegers, G. C. Dismukes and L. Spiccia, *Angew. Chem., Int. Ed.*, 2008, **47**, 7335.
24 M. M. Najafpour, S. Nayeri and B. Pashaei, *Dalton Trans.*, 2011, **40**, 9374.
25 J. J. Concepcion, J. W. Jurss, M. K. Brennaman, P. G. Hoertz, A. O. T. Patrocinio, N. Y. Murakami Iha, J. L. Templeton and T. J. Meyer, *Acc. Chem. Res.*, 2009, **42**, 1954.
26 D. Shevchenko, M. F. Anderlund, A. Thapper and S. Styring, *Energy Environ. Sci.*, 2011, **4**, 1284.
27 A. Harriman, I. J. Pickering, J. M. Thomas and P. A. Christensen, *J. Chem. Soc., Faraday Trans. 1*, 1988, **84**, 2795.
28 T. Nakagawa, C. A. Beasley and R. W. Murray, *J. Phys. Chem. C*, 2009, **113**, 12958.
29 T. Nakagawa, N. S. Bjorge and R. W. Murray, *J. Am. Chem. Soc.*, 2009, **131**, 15578.
30 R. Cao, H. Y. Ma, Y. V. Geletii, K. I. Hardcastle and C. L. Hill, *Inorg. Chem.*, 2009, **48**, 5596.
31 M. Risch, V. Khare, I. Zaharieva, L. Gerencser, P. Chernev and H. Dau, *J. Am. Chem. Soc.*, 2009, **131**, 6936.
32 L. Duan, Y. H. Xu, M. Gorlov, L. P. Tong, S. Andersson and L. C. Sun, *Chem.–Eur. J.*, 2010, **16**, 4659.
33 Y. H. Xu, L. L. Duan, L. P. Tong, B. Åkermark and L. C. Sun, *Chem. Commun.*, 2010, **46**, 6506.
34 L. Duan, A. Fischer, Y. H. Xu and L. C. Sun, *J. Am. Chem. Soc.*, 2009, **131**, 10397.
35 Y. H. Xu, T. Åkermark, V. Gyollai, D. P. Zou, L. Eriksson, L. L. Duan, R. Zhang, B. Åkermark and L. C. Sun, *Inorg. Chem.*, 2009, **48**, 2717.
36 W. C. Ellis, N. D. McDaniel, S. Bernhard and T. J. Collins, *J. Am. Chem. Soc.*, 2010, **132**, 10990.
37 J. L. Fillol, Z. Codolá, I. Garcia-Bosch, L. Gómez, J. J. Pla and M. Costas, *Nat. Chem.*, 2011, **3**, 807.
38 P. G. Hoertz, Y. I. Kim, W. J. Youngblood and T. E. Mallouk, *J. Phys. Chem. B*, 2007, **111**, 6845.
39 N. D. Morris, M. Suzuki and T. E. Mallouk, *J. Phys. Chem. A*, 2004, **108**, 9115.
40 N. D. Morris and T. E. Mallouk, *J. Am. Chem. Soc.*, 2002, **124**, 11114.
41 M. Hara, C. C. Waraksa, J. T. Lean, B. A. Lewis and T. E. Mallouk, *J. Phys. Chem. A*, 2000, **104**, 5275.
42 M. Yagi, M. Toda, S. Yamada and H. Yamazaki, *Chem. Commun.*, 2010, **46**, 8594.
43 M. Yagi and K. Narita, *J. Am. Chem. Soc.*, 2004, **126**, 8084.
44 N. D. McDaniel, F. J. Coughlin, L. L. Tinker and S. Bernhard, *J. Am. Chem. Soc.*, 2008, **130**, 210.
45 S. Fukuzumi, S. Kato and T. Suenobu, *Phys. Chem. Chem. Phys.*, 2011, **13**, 17960.

46 A. K. Poulsen, A. Rompel and C. J. McKenzie, *Angew. Chem., Int. Ed.*, 2005, **44**, 6916.
47 Y. Gao, T. Åkermark, J. H. Liu, L. C. Sun and B. Åkermark, *J. Am. Chem. Soc.*, 2009, **131**, 8726.
48 Y. V. Geletii, B. Botar, P. Koegerler, D. A. Hillesheim, D. G. Musaev and C. L. Hill, *Angew. Chem., Int. Ed.*, 2008, **47**, 3896.
49 Y. V. Geletii, C. Besson, Y. Hou, Q. S. Yin, D. G. Musaev, D. Quinonero, R. Cao, K. I. Hardcastle, A. Proust, P. Kogerler and C. L. Hill, *J. Am. Chem. Soc.*, 2009, **131**, 17360.
50 A. Sartorel, M. Carraro, G. Scorrano, R. De Zorzi, S. Geremia, N. D. McDaniel, S. Bernhard and M. Bonchio, *J. Am. Chem. Soc.*, 2008, **130**, 5006.
51 M. Murakami, D. Hong, T. Suenobu, S. Yamaguchi, T. Ogura and S. Fukuzumi, *J. Am. Chem. Soc.*, 2011, **133**, 11605.
52 S. W. Gersten, G. J. Samuels and T. J. Meyer, *J. Am. Chem. Soc.*, 1982, **104**, 4029.
53 J. J. Concepcion, M. K. Tsai, J. T. Muckerman and T. J. Meyer, *J. Am. Chem. Soc.*, 2010, **132**, 1545.
54 J. J. Concepcion, J. W. Jurss, M. R. Norris, Z. F. Chen, J. L. Templeton and T. J. Meyer, *Inorg. Chem.*, 2010, **49**, 1277.
55 R. Zong and R. P. Thummel, *J. Am. Chem. Soc.*, 2005, **127**, 12802.
56 H. W. Tseng, R. Zong, J. T. Muckerman and R. Thummel, *Inorg. Chem.*, 2008, **47**, 11763.
57 J. T. Muckerman, D. E. Polyansky, T. Wada, K. Tanaka and E. Fujita, *Inorg. Chem.*, 2008, **47**, 1787.
58 Z. F. Chen, J. J. Concepcion, J. W. Jurss and T. J. Meyer, *J. Am. Chem. Soc.*, 2009, **131**, 15580.
59 J. J. Concepcion, J. W. Jurss, J. L. Templeton and T. J. Meyer, *J. Am. Chem. Soc.*, 2008, **130**, 16462.
60 D. J. Wasylenko, C. Ganesamoorthy, M. A. Henderson, B. D. Koivisto, H. D. Osthoff and C. P. Berlinguette, *J. Am. Chem. Soc.*, 2010, **132**, 16094.
61 D. J. Wasylenko, C. Ganesamoorthy, B. D. Koivisto, M. A. Henderson and C. P. Berlinguette, *Inorg. Chem.*, 2010, **49**, 2202.
62 S. Romain, F. Bozoglian, X. Sala and A. Llobet, *J. Am. Chem. Soc.*, 2009, **131**, 2768.
63 L. Bernet, R. Lalrempuia, W. Ghattas, H. Mueller-Bunz, L. Vigara, A. Llobet and M. Albrecht, *Chem. Commun.*, 2011, **47**, 8058.
64 D. E. Polyansky, J. T. Muckerman, J. Rochford, R. Zong, R. P. Thummel and E. Fujita, *J. Am. Chem. Soc.*, 2011, **133**, 14649.
65 Y. Xu, A. Fischer, L. Duan, L. Tong, E. Gabrielsson, B. Åkermark and L. Sun, *Angew. Chem., Int. Ed.*, 2010, **49**, 8934.
66 H. Yamada, W. F. Siems, T. Koike and J. K. Hurst, *J. Am. Chem. Soc.*, 2004, **126**, 9786.
67 D. Hong, M. Murakami, Y. Yamada and S. Fukuzumi, *Energy Environ. Sci.*, 2012, **5**, 5708.
68 F. Bozoglian, S. Romain, M. Z. Ertem, T. K. Todorova, C. Sens, J. Mola, M. Rodriguez, I. Romero, J. Benet-Buchholz, X. Fontrodona, C. J. Cramer, L. Gagliardi and A. Llobet, *J. Am. Chem. Soc.*, 2009, **131**, 15176.
69 J. D. Blakemore, N. D. Schley, D. Balcells, J. F. Hull, G. W. Olack, C. D. Incarvito, O. Eisenstein, G. W. Brudvig and R. H. Crabtree, *J. Am. Chem. Soc.*, 2010, **132**, 16017.
70 R. Lalrempuia, N. D. McDaniel, H. Muller-Bunz, S. Bernhard and M. Albrecht, *Angew. Chem., Int. Ed.*, 2010, **49**, 9765.
71 A. Savini, G. Bellachioma, G. Ciancaleoni, C. Zuccaccia, D. Zuccaccia and A. Macchioni, *Chem. Commun.*, 2010, **46**, 9218.
72 A. Savini, P. Belanzoni, G. Bellachioma, C. Zuccaccia, D. Zuccaccia and A. Macchioni, *Green Chem.*, 2011, **13**, 3360.
73 D. G. H. Hetterscheid and J. N. H. Reek, *Chem. Commun.*, 2011, **47**, 2712.
74 G. W. Brudvig, J. D. Blakemore, N. D. Schley, G. W. Olack, C. D. Incarvito and R. H. Crabtree, *Chem. Sci.*, 2011, **2**, 94.
75 D. Shevchenko, M. F. Anderlund, A. Thapper and S. Styring, *Energy Environ. Sci.*, 2011, **4**, 1284.
76 F. Jiao and H. Frei, *Angew. Chem., Int. Ed.*, 2009, **48**, 1841.
77 B. S. Brunschwig, M. H. Chou, C. Creutz, P. Ghosh and N. Sutin, *J. Am. Chem. Soc.*, 1983, **105**, 4832.
78 P. K. Ghosh, B. S. Brunschwig, M. Chou, C. Creutz and N. Sutin, *J. Am. Chem. Soc.*, 1984, **106**, 4772.
79 C. Creutz and N. Sutin, *Proc. Natl. Acad. Sci. U. S. A.*, 1975, **72**, 2858.
80 G. L. Elizarova, L. G. Matvienko and V. N. Parmon, *J. Mol. Catal.*, 1987, **43**, 171.
81 Y. Surendranath, M. W. Kanan and D. G. Nocera, *J. Am. Chem. Soc.*, 2010, **132**, 16501.
82 J. B. Gerken, J. G. McAlpin, J. Y. C. Chen, M. L. Rigsby, W. H. Casey, R. D. Britt and S. S. Stahl, *J. Am. Chem. Soc.*, 2011, **133**, 14431.
83 Z. Huang, Z. Luo, Y. V. Geletii, J. W. Vickers, Q. Yin, D. Wu, Y. Hou, Y. Ding, J. Song, D. G. Musaev, C. L. Hill and T. Lian, *J. Am. Chem. Soc.*, 2011, **133**, 2068.
84 Q. S. Yin, J. M. Tan, C. Besson, Y. V. Geletii, D. G. Musaev, A. E. Kuznetsov, Z. Luo, K. I. Hardcastle and C. L. Hill, *Science*, 2010, **328**, 342.
85 J. J. Stracke and R. G. Finke, *J. Am. Chem. Soc.*, 2011, **133**, 14872.
86 G. C. Dismukes, N. S. McCool, D. M. Robinson and J. E. Sheats, *J. Am. Chem. Soc.*, 2011, **133**, 11446.
87 M. Ciampoli and N. Nardi, *Inorg. Chem.*, 1966, **5**, 41.
88 G. J. P. Britovsek, J. England and A. J. P. White, *Inorg. Chem.*, 2005, **44**, 8125.
89 Y. J. Choi, K. B. Cho, M. Kubo, T. Ogura, K. D. Karlin, J. Cho and W. Nam, *Dalton Trans.*, 2011, **40**, 2234.
90 U. Kolle and B. Fuss, *Chem. Ber.*, 1984, **117**, 743.
91 L. Dadci, H. Elias, U. Frey, A. Hornig, U. Koelle, A. E. Merbach, H. Paulus and J. S. Schneider, *Inorg. Chem.*, 1995, **34**, 306.
92 Y. M. Dong, K. He, L. Yin and A. M. Zhang, *Nanotechnology*, 2007, **18**, 435602.
93 Y. Yamada, K. Yano, Q. A. Xu and S. Fukuzumi, *J. Phys. Chem. C*, 2010, **114**, 16456.
94 J. Cho, R. Sarangi, H. Y. Kang, J. Y. Lee, M. Kubo, T. Ogura, E. I. Solomon and W. Nam, *J. Am. Chem. Soc.*, 2010, **132**, 16977.
95 H. S. White, W. G. Becker and A. J. Bard, *J. Phys. Chem.*, 1984, **88**, 1840.
96 A. L. Kaledin, Z. Huang, Y. V. Geletii, T. Lian, C. L. Hill and D. G. Musaev, *J. Phys. Chem. A*, 2010, **114**, 73.
97 The concentration effect of $[Ru(bpy)_3]^{2+}$ on O_2 yield in the photocatalytic water oxidation in the presence of precatalyst **1** is depicted in Fig. S9 in ESI†.
98 L. H. Hu, Q. Peng and Y. D. Li, *J. Am. Chem. Soc.*, 2008, **130**, 16136.
99 J. Yang, H. Liu, W. N. Martens and R. L. Frost, *J. Phys. Chem. C*, 2010, **114**, 111.

